Magnetic Resonance Imaging 60 (2019) 164–172

Contents lists available at ScienceDirect

Magnetic Resonance Imaging

journal homepage: www.elsevier.com/locate/mri

Original contribution

Non-contrast-enhanced magnetic resonance imaging for visualization and quantification of endovascular aortic prosthesis, their endoleaks and aneurysm sacs at 1.5 T

Mona Salehi Ravesh[a,b,*,1], Patrick Langguth[b,1], Julian Andreas Pfarr[b], Jasper Schupp[b], Jens Trentmann[b], Ioannis Koktzoglou[c,d], Robert R. Edelman[c,e], Joachim Graessner[f], Andreas Greiser[g], David Hautemann[h], Anja Hennemuth[i], Marcus Both[b], Olav Jansen[b], Jan-Bernd Hövener[a], Jost Philipp Schäfer[b]

[a] Section Biomedical Imaging, Molecular Imaging North Competence Center (MOIN CC), Department of Radiology and Neuroradiology, University Medical Center Schleswig-Holstein (UKSH), Kiel University, Kiel, Germany
[b] Department of Radiology and Neuroradiology, University Medical Center Schleswig-Holstein (UKSH), Kiel University, Kiel, Germany
[c] Department of Radiology, NorthShore University HealthSystem, Evanston, IL, USA
[d] University of Chicago Pritzker School of Medicine, Chicago, IL, USA
[e] Northwestern University Feinberg School of Medicine, Chicago, IL, USA
[f] Siemens Healthcare GmbH, Hamburg, Germany
[g] Siemens Healthcare GmbH, Erlangen, Germany
[h] Medis Medical Imaging Systems BV, Leiden, the Netherlands
[i] Fraunhofer Mevis, Bremen, Germany

ARTICLE INFO

Keywords:
Endovascular aortic aneurysm repair (EVAR)
Magnetic resonance imaging (MRI)
4-Dimensional phase contrast flow magnetic resonance imaging (4D flow MRI)
Quiescent-interval single-shot (QISS)
MR angiography (MRA)
T_1-mapping
T_2-mapping

ABSTRACT

Purpose: After an endovascular aortic aneurysm repair (EVAR), a follow-up at 1, 6 and every 12 months is recommended for remainder of the patient's life. The diagnostic standard methods for diagnosing endoleaks and visualization of aneurysms in EVAR-patients are: invasive digital subtraction angiography (DSA), contrast enhanced (CE) computed tomographic angiography (CE-CTA), and magnetic resonance angiography (CE-MRA). These techniques, however, require the use of iodine- or gadolinium-based contrast agents with rare, but possibly life threatening side effects such as renal impairment, thyrotoxicosis and allergic reactions, nephrogenic systemic fibrosis, and cerebral gadolinium deposition. The aim of this prospective study was to compare a non-contrast-enhanced MRI protocol (consist of four MRI methods) with DSA and CE-CTA for visualization and quantification of endovascular aortic prosthesis, their endoleaks and aneurysms.

Material and methods: Eight patients (mean age 76.8 ± 4.9 years, 63% male), whose thoracic, abdominal, or iliac aneurysms were treated with different endovascular prosthesis and suffered from type I–V endoleaks, were examined on a 1.5 Tesla MR system. Quiescent-interval slice selective MR angiography (QISS-MRA), 4-dimensional (4D)-flow MRI, T_1- and T_2-mapping, as well as DSA and CE-CTA were used for the visualization and quantification of endoprosthesis, endoleaks, and aneurysms in these patients.

Results: QISS-MRA provided good visualization of endoleaks and comparable quantification of aneurysm size with respect to CE-CTA and DSA. The 4D-flow MRI provided additional information about the wall shear stress, which could not be determined using DSA. In contrast to CE-CTA, T_1- and T_2-mapping provided detailed information about heterogeneous areas within an aneurysm sac.

Conclusions: Compared to DSA and CE-CTA, the proposed MRI methods provide improved anatomical and functional information for various types of endoprostheses and endoleaks. In addition, hemodynamic parameters

* Corresponding author at: Department of Radiology and Neuroradiology, University Medical Center Schleswig-Holstein (UKSH), Kiel University, Arnold Heller Street 3, Building 41, 24105 Kiel, Germany.
E-mail address: Mona.Salehiravesh@uksh.de (M. Salehi Ravesh).
[1] Dr. Mona Salehi Ravesh and Dr. Patrick Langguth contributed equally to this work.

https://doi.org/10.1016/j.mri.2019.05.012
Received 20 December 2018; Received in revised form 7 April 2019; Accepted 4 May 2019

of the aorta and information on the content of aneurysm sac are provided as well. Within the frame of personalized medicine, the personalized diagnosis enabled by this non-CE MRI protocol is the foundation for a personalized and successful treatment.

1. Introduction

Endovascular aortic aneurysm repair (EVAR) using transcatheter-deployed stent-grafts is a minimally invasive interventional technique alternative to open surgical aortic repair [1]. Remaining perfusion of the aneurysmatic segment via leakage is called endoleak. Generally, there are five types (I–V) of endoleaks [2,3].

After the implantation of an endoprosthesis, a series of follow-up imaging examinations [4] are normally performed to 1) confirm the position of the prosthesis in the vessel, whether the prosthesis is folded, whether there is an infection and stenosis in the prosthesis, or whether the prosthesis material has a defect, 2) to determine, whether there is an evidence for the presence of an endoleak, and 3) in case of an aneurysm, to monitor the anatomical evolution of the aneurysm in terms of size and content over time.

Invasive digital subtraction angiography (DSA), contrast enhanced computed tomographic angiography (CE-CTA), CE magnetic resonance angiography (CE-MRA) are standard procedures to answer the above mentioned questions [5,6]. These techniques, however, require the use of iodine- or gadolinium-based contrast agents with rare, but possibly life threatening side effects such as renal impairment, thyrotoxicosis and allergic reactions, nephrogenic systemic fibrosis, cerebral gadolinium deposition [7,8]. Thus, a non-invasive and non-CE imaging approach that also avoids ionizing radiation would be beneficial for the safety of the patient.

Contrast-enhanced ultrasound (CE-US) is a relatively new, cost effective and minimally invasive modality in detection of endoleaks [9], like most ultrasound techniques, however, it is investigator dependent and sometimes difficult in reproducibility.

Fortunately, MRI offers a variety of non-CE techniques, which can be used for anatomical and functional characterization of vessels and aneurysms. Edelman et al. reported about a 2D electro-cardio-gram (ECG)-triggered MRA technique (quiescent-interval slice-selective, QISS) with a radial k-space sampling for the visualization of the pulmonary and coronary arteries [10,11]. In addition, time-resolved phase contrast MR imaging with blood flow velocity encoding along three-dimensional spatial directions (4D-flow MRI [12]) has emerged as a promising technique, that provides a comprehensive visualization of the aortic hemodynamics and also retrospective quantification of its hemodynamic parameters [13,14]. Moreover, mapping of the longitudinal (T_1) and transversal (T_2) magnetization relaxation times can be used for characterization of aneurysmal contents.

The aim of this prospective study was to compare a non-contrast-enhanced MRI protocol consisting of four MRI methods with DSA and CE-CTA for visualization and quantification of endovascular aortic prosthesis, their endoleaks and the contents of the aneurysmal sacs.

2. Material and methods

In this prospective study, patients were included, who had been treated using an endovascular prosthesis due to their thoracic, abdominal, or iliac aneurysms in our center from February to August 2018. This study was performed according to the protocol (No. D 517/18) approved by the institutional ethics committee and in accordance with the ethical standards laid down in the 1964 declaration of Helsinki and its later amendments. All study participants gave their informed consent in a written form.

The focus of the patient selection was to recruit of at least one patient for each of known endoleak types. Our patient selection covered a wide range of endoleaks: post-interventional types I and II, newly-emerged type I, type III and type IV. Cases presenting as technically and clinically complex, leading to an aneurysm growth, were included as well. In the following part, only the most relevant patient history that prompted diagnostic imaging is provided.

The first patient had a folded thoracic EVAR (TEVAR) in the aortic arch, endoleak type Ia and II due to the insufficient embolization of subclavian artery, and a penetrating aortic ulcer (PAU) treated with several coil embolizations. The influence of the TEVAR stenosis on the blood flow pattern in the endoprosthesis was investigated.

The second patient had a large, recently implanted TEVAR from aortic arch into thoracic aorta with an atypical PAU in the aortic arch. He was examined after the coil embolization of his PAU and the brachiocephalic artery in order to clarify whether he had a residual perfusion of his PAU, probably due to type II endoleak via the vasa vasorum.

An infrarenal Y-shaped prosthesis with bilateral iliac side branches was implanted in the third patient. During the intervention, a significant, probably endoleak type Ib or II was observed, which was perfused via the right iliac artery. Further examination using CT and MRI was planned for a detailed investigation of the cause of the endoleak and before an embolization process.

A fourth patient with a thoracic and abdominal EVAR with known endoleaks type Ib and II was examined due to enlargement of his aneurysm sac over the course of two months.

The fifth patient had a thoracic and abdominal endoprosthesis with side branches in all four visceral arteries (celiac trunk, superior mesenteric artery (SMA) and renal arteries). The presumption for the presence of an endoleak type III at the fenestration of the celiac trunk in a dislocated branch or a still perfused endoleak type II was investigated. Moreover, the reason for the markedly perfused false lumen in the thoracic aorta needed to be clarified.

The aneurysm sac of the sixth patient was continuously growing over the time, although three overlapping thoracic and abdominal endoprostheses were implanted in this patient. The position of the suspected type III endoleak needed to be found.

The seventh patient had a thoracic endoprosthesis and an abdominal endoprosthesis. These were surrounded with large and growing aneurysm sacs. In this patient, the endoleak was classified as type IV due to a material defect of the implanted fenestrated EVAR (FEVAR). The size and the contents of the aneurysmal sacs needed to be evaluated.

The eighth patient had an aortobiiliac EVAR with a large and well perfused aneurysm sac. The physiological status of the endoleak could not be classified according to the known endoleak types I–V. A new type of endoleak was suspected.

Detailed information about the implanted endoprosthesis in this work are available in the supplement.

2.1. Non-invasive MR imaging and analysis

Imaging was performed on a 1.5 Tesla MRI system (Magnetom Aera, XQ gradients, Siemens Healthcare, Erlangen, Germany) using an 18-channel torso coil (Siemens Healthcare, Erlangen, Germany). Following fast gradient-echo imaging of three orthogonal slices, depending on the clinical question, QISS-MRA, 4D-flow MRI, and T_1- and T_2-mapping were performed with the parameters in Table 1.

QISS is a 2D cardiac-gated non-CE MRA technique that suppresses stationary tissue, allows a time period for arterial inflow, and uses a balanced steady state free precession (bSSFP) readout. The original implementation of QISS-MRA, designed for evaluating the peripheral

Table 1
MR protocol parameters used in this study. The repetition time is abbreviated to TR, echo time, to TE, band width to BW, flip angle to FA, generalized autocalibrating partially parallel acquisition to GRAPPA.

Parameters/ sequence	TR/TE (ms)	Acquisition matrix	Reconstructed voxel size (mm^3)	BW (Hz/Px)	Number of slices	Distance factor (%)	FA (°)	GRAPPA acceleration factor/reference line	Other	Total acquisition time (min:s) depending on the heart rate
QISS-MRA	993.9/1.7	318 × 318	1.1 × 1.1 × 2.5	1359	59	−20	120	–	– Radial balanced steady-state free precession (bSSFP) readout views: 200 – Chemical shift-selective fat suppression – Thickness of in-plane inversion using a frequency offset corrected inversion (FOCI) radio-frequency (RF) pulse: 3.75 mms – Time from in-plane and venous saturation to acquisition of central k-space (TI): 650 ms – Trigger delay (TD): 0 ms – bSSFP repetition time: 3.4 ms	1:00
4D flow	40.6/2.3	160 × 86	2.4 × 2.4 × 2.5	453	28	0	7	2/32	Temporal resolution: 40.6 ms; VENC: 150 cm/s	6:34
T_1-map	285.5/1.0	250 × 163	1.8 × 1.8 × 8.0	1085	5	0	35	2/36	Inversion times: 100 and 180 ms	1.50–2.00
T_2-map	323.8/1.1	250 × 163	1.8 × 1.8 × 8.0	1149	5	0	70	2/36	Three T_2 preparation times: 0, 25 and 55 ms	1.50–2:00

vessels, used a Cartesian readout [15]. In this study, a QISS-MRA with radial k-space sampling was used, which is less sensitive to motion and pulsation artefacts [10,16]. In radial QISS MRA, an in-plane frequency-offset corrected inversion (FOCI) pulse is applied immediately after the R-wave to suppress background signal. After this pulse, a quiescent interval (QI) of approximately 300 ms is applied to allow fresh and fully magnetized blood to enter the imaging slice. A frequency-selective fat-suppression pulse is applied next to suppress the signal from fat, which has recovered during the QI. Finally, the QISS slice is acquired using a 2D-single shot radial bSSFP readout. QISS-MRA performs best when the imaging slices are positioned approximately perpendicular to the target vessels. The QISS-MRA data set was acquired in coronal and axial views with prospective ECG-gating under free-breathing conditions.

T_1- and T_2-mapping are two contrast agent-free MRI techniques, which are used mainly in cardiac MRI for determination of myocardial fibrosis (short T_1-time) [17] or edema (long T_2-time) [18]. In the last years, these methods were increasingly used for the characterization of other tissue types, such as brain, liver and prostate, in which the tissue composition becomes heterogeneous due to various diseases [19]. In patients with continuously growing aneurysms, it is important to figure out the reason for the growth first. Secondly, it is clinically relevant to quantify the tissue types of the aneurysm sac, in order to plan an appropriate strategy for the treatment or re-intervention. The ECG-triggered T_1- and T_2-mapping of the thoracic and abdominal aortic aneurysm were obtained in a single breath-hold per slice using a modified Look-Locker (MOLLI) prototype sequence and a T_2 preparation technique (Table 1). The T_1- and T_2-mapping were acquired in coronal and axial views. To cover large aneurysms, imaging was divided into two or three parts, such that the breath-holding time per image segment was shortened. The T_1- and T_2-mapping sequences were repeated for these segments in succession.

The T_1- and T_2-maps were created using a dedicated commercial software (Module QStrain in MedisSuite MR, version 3.0, Medis Medical Imaging Systems BV, Leiden, The Netherlands).

4D-flow MRI was introduced in 2003 by Wigstrom et al. [20]. Since then, this contrast-agent free method has been used to visualize and quantify the hemodynamics of various vessels, especially in the different sections of aorta [21]. Here, 4D-flow MRI was performed using a prototype sequence with prospective ECG-gating during free-breathing using a respiratory navigator. The acquired volume was oriented along an oblique sagittal plane encompassing the ascending aorta, the aortic arch, and the thoracic aorta (Table 1). The 3D visualization of aorta, the quantification of the flow velocity and wall shear stress (WSS) in the aorta were performed using a commercially available software package (GTFlow, GyroTools, LLC, Zurich, Switzerland). The relative blood pressure of different aortic segments was calculated and visualized (MevisFlow, version 10.3, Fraunhofer MEVIS, Bremen, Germany).

2.2. Invasive angiography

Interventional procedures in all patients were performed on an angiography system (Artis Zeego, Siemens Healthcare, Erlangen, Germany). The procedure was usually performed in general anesthesia. Percutaneous approach involved groin puncture on both sides after local disinfection and under sterile conditions. In some cases, especially in visceral fenestrated/branched EVAR, a cubital puncture of the brachial artery was necessary. Implantation of the main body of the prosthesis were made via a 20–24F sheath, iliac bodies were implanted via a 12–14F sheath. Otherwise a 5F sheath for diagnostic catheters was used on the other side. In case of the implantation of visceral branches in FEVARs, a 6–8F sheath was used for cubital access. The procedures were performed with use of percutaneous suture systems (Perclose Proglide, Abbot Vascular, Illinois, USA) and vascular closure device (AngioSeal, Terumo, Tokyo, Japan) for groin access and manual compression for cubital access. For periprocedural navigating DSA and fluoroscopic scenes were performed. Iodine contrast agent was used

(Imeron 350, Bracco Imaging, Milano, Italy). Intravenous antibiotic prophylaxes (1.5 g cefuroxime) were given praeprocedural.

2.3. Non-/minimal-invasive CT

Thoracic and abdominal images were acquired using a dual-source 128-row CT system (SOMATOM Definition Flash, Siemens Healthcare, Forchheim, Germany) with following protocol parameters: tube voltage: 100 kV, tube current time product: 59 mAs, slice collimation: 2.0 × 128 × 0.6 mm, rotation time: 0.5 s, spiral pitch factor: 1.2. A maximum intensity projections (MIPs) of the CT data sets were created.

2.4. Data analysis

All patients were examined using both invasive and minimal/non-invasive DSA, CE-CTA, and MRA techniques. All images were evaluated based on a consensus decision between three board-certified radiologists (P. L., J.A. P., J.P. S.) with at least 5 to 15 years of experience in intervention.

Our pilot study was conducted to proof the feasibility of the tested MRI methods in endoleak visualization and classification at all. In general, the evaluation between all three imaging modalities was focused on three common aspects within this patient cohort: 1) visualization (localization) of different endoleak types and the clarity of the reason for their emergence, 2) size of aneurysm, and 3) heterogeneity of aneurysm content.

3. Results

A total of eight patients (63% male, mean age 76.8 ± 4.9 years, mean weight 79.9 ± 12.2 kg) were included in this study.

3.1. Utility of QISS-MRA

The comparability of CE-CTA and non-CE QISS-MRA was investigated for the visualization of endoprosthesis and detection of various types of endoleaks (Fig. 1).

In patient no. 6, the persistent re-entry as a connection between the inner prosthetic and outer prosthetic lumen was visualized identically using CE-CTA and QISS-MRA (red arrows). The stent struts on the CE-CTA were hyperdense, whereas they were hypointense on QISS-MRA (Fig. 1a). The implants did not cause other obvious artefacts. In patient no. 4, the perfused area of the aneurysm sac was clearly demarcated on the early arterial phase post-contrast CTA and non-CE QISS-MRA images (red arrows). The content of the retro-cardiac aneurysm sac on the CE-CTA appeared homogenous and non-perfused. In contrast to that, the QISS-MRA showed an almost completely perfused volume (Fig. 1b). In patient no. 5, CE-CTA showed contrast enhancement in the endoprosthesis (blue arrows) and also in the aneurysm sac (red arrows). A similar signal was observed by QISS-MRA without contrast agent (Fig. 1c). In patient no. 7, the two red arrows point at the perfused aneurysm sac, which was pronounced both in the thoracic and also in the abdominal part of the endoprosthesis (Fig. 1d).

3.2. Utility of 4D-flow MRI

The invasive angiography was compared with non-invasive MRI for the assessment of the hemodynamics in the endoprosthesis (Fig. 2).

The invasive angiographic image (Fig. 2aI) showed the unmodified folded shape of the TEVAR-endoprosthesis in the aortic arch after coil embolization of the endoleak type Ia, II and PAU in patient no. 1. In the DSA image (Fig. 2aII), there was a flow delay at the narrowed segment of the TEVAR-endoprosthesis in the aortic arch. No difference in blood pressure was found by catheter measurements before, within and after the stenosis. The mean arterial blood pressure value was 105 mmHg (150/70 mmHg). As before, no artefacts were apparent on the 4D-flow MRI, even within the prosthesis. In Fig. 2aIII, the segments 1, 2 and 3 show the beginning, the narrowest part, and the end of the TEVAR-endoprosthesis on a 3D reconstruction from a non-CE 4D-flow MRI data set. From this data, a time-resolved relative pressure in the aorta was calculated with respect to segment 2. A small difference in blood pressure of 3–5 mmHg was found between segments 1 and 3, which is

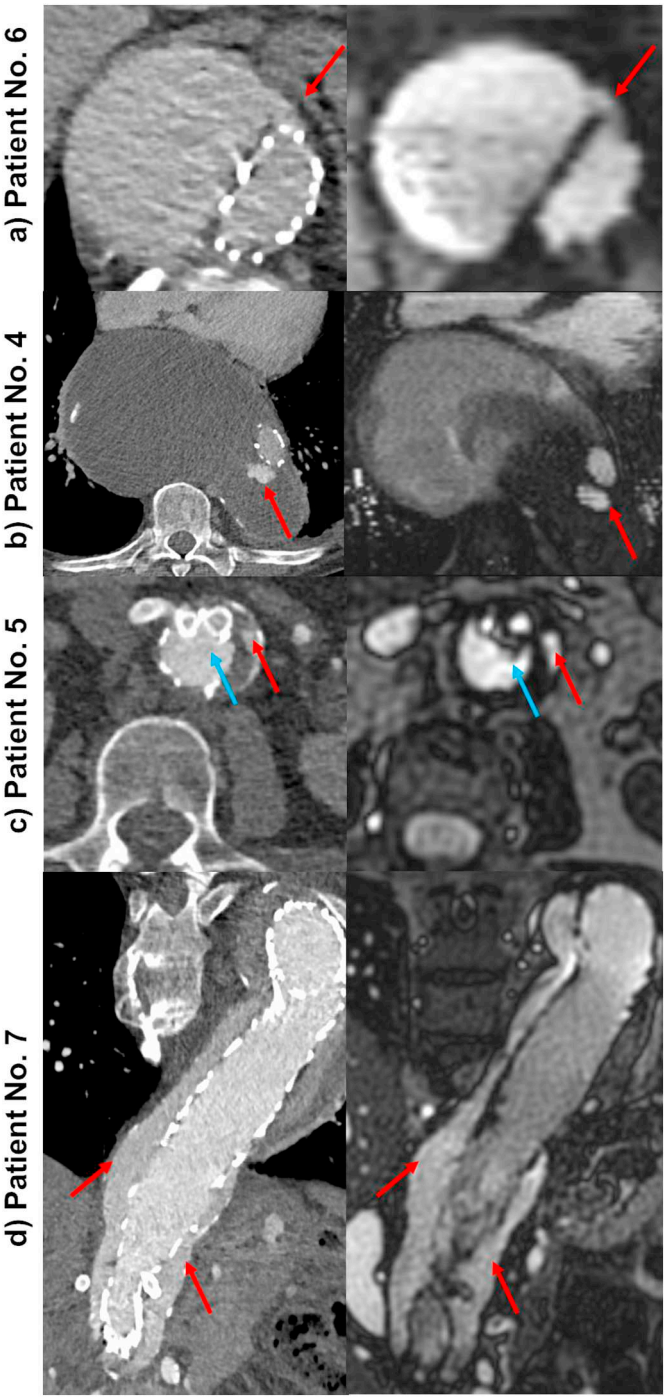

Fig. 1. Comparison between CE-CTA (left) and non-CE QISS-MRA (right) concerning the visualization of various types of endoprosthesis and detection of endoleaks. The endoprostheses are visible with little metallic image artefacts on the reconstructed maximum intensity projection (MIP) CE-CTA and QISS-MRA images. Red arrows indicate the perfused parts of aneurysm sacs and blue arrow the contrast enhancement in the endoprosthesis. (For interpretation of the references to color in this figure legend, the reader is referred to the web version of this article.)

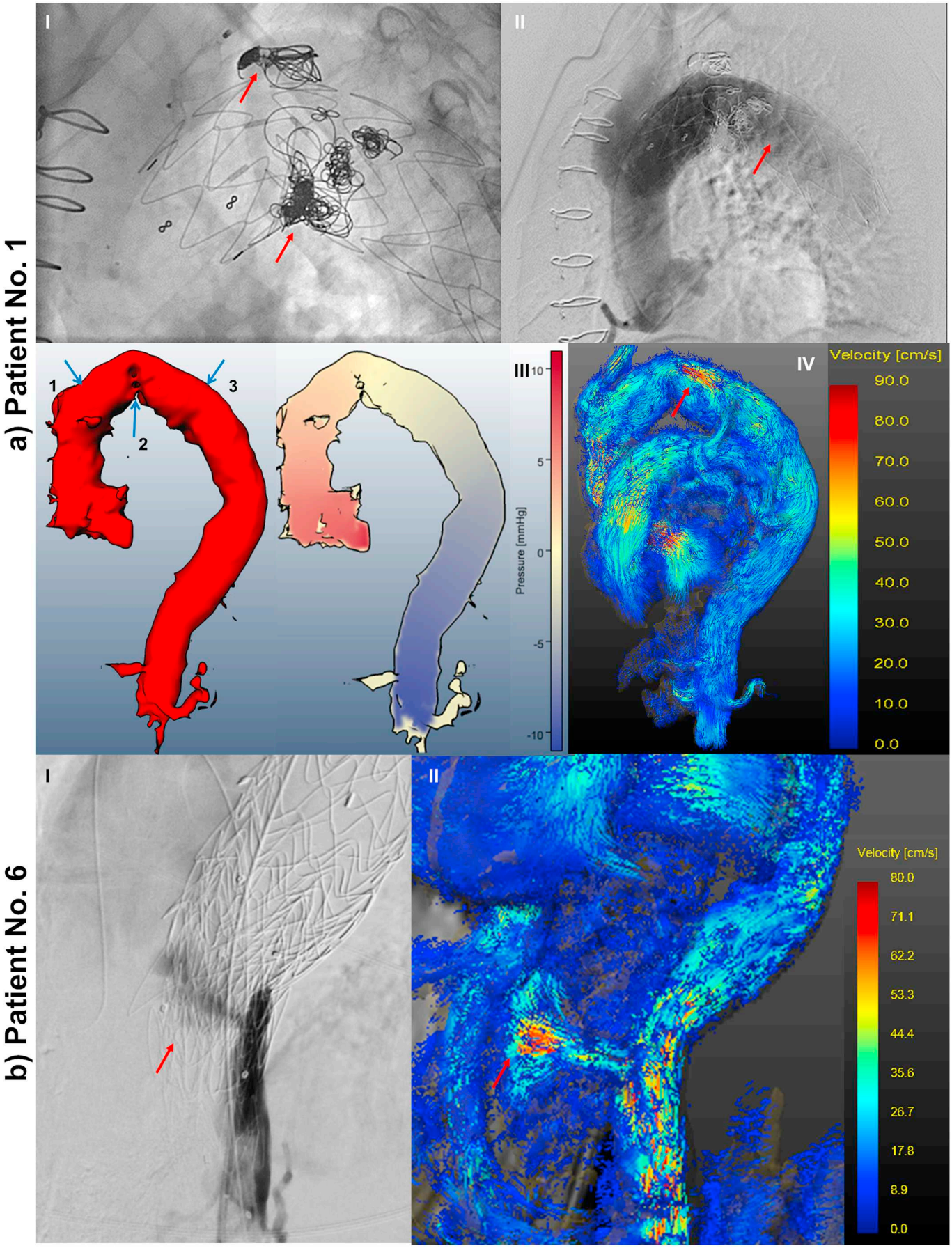

(caption on next page)

Fig. 2. Comparison between the DSA and 4D-flow MRI for the assessment of the hemodynamics in the endoprosthesis of two patients. The narrowing in the aortic arch was identified on invasive angiography images and the 3D reconstruction (a, I, II and III). 4D-flow MRI was acquired and used to reconstruct the 3D volume of the aorta, a relative pressure map (III) and the flow velocity path lines (IV). Three segments of the aorta were identified, correspond to the beginning (1), the narrowing (2), and the end (3) of the TEVAR-endoprosthesis. The determined blood pressure difference between the segments 1 and 3 was not clinically relevant and this result was confirmed by invasive measurement. An accelerated flow in segment 2 was observed by 4D-flow MRI. A jet into the aneurysm sac was found by DSA and 4D-flow MRI (b, I, II, red arrow). (For interpretation of the references to color in this figure legend, the reader is referred to the web version of this article.)

clinically not relevant. The flow acceleration at the narrowed segment 2 was clearly visualized on a color-coded path-lines map of the blood flow velocity in the aorta (Fig. 2aIV). Two hemodynamically relevant parameters (WSS and blood flow velocity) at these segments are listed in Table 2. The accelerated blood flow at the re-entry connection point between the inner prosthetic and outer prosthetic lumen of the abdominal endoprosthesis in patient no. 6 with an endoleak type III (Fig. 2bI, see transversal view in Fig. 1a) was visualized on both invasive angiography and non-CE 4D-flow MRI (Fig. 2bII, red arrow).

Note that the number of images for patient no. 1 and no. 6 is different, because of different clinical questions.

3.3. Utility of T_1- and T_2-mapping MRI

The aneurysm sacs with increasing size over the time usually had a heterogeneous texture, which consisted of a mixture of whole blood, blood sediment, blood plasma, and possibly interventional embolization materials. CE-CTA was compared to MRI with respect to the content of the aneurysm sac (Fig. 3).

In patient no. 8, the grey scaled CE-CTA images allowed to distinguish between the solid and liquid components of the aneurysm sac, as long as there were no image artefacts due to the embolization materials (Fig. 3a). CE-T_1 weighted MRI provided more detailed information than CE-CTA, including texture of the aneurysm sac and its perfusion. The lower signal intensity in the "starlike" regions in the middle of the aneurysm sac indicated a lower perfusion compared to the other parts of aneurysm with a higher signal intensity. A pixel-wise analysis of the aneurysm content using non-CE T_1- and T_2-maps confirmed this heterogeneity of the texture within the aneurysm sac. The T_1- and T_2-values were color-coded within a range from 200 to 1800 ms (Fig. 3a) and from 0 to 2500 (Fig. 3b and c) for T_1, and from 0 to 200 for T_2 (Fig. 3a), depending on the aneurysm content. To interpret these maps, results published elsewhere were used (samples at 1.5 T, T_1/T_2: whole blood: 1582 ± 69/254 ± 26 ms, blood sediment: 990 ± 53/137 ± 9 ms, blood plasma: 2277 ± 67/416 ± 77 ms [22,23]). In patient no. 7, flowing blood (Fig. 3b, I) and clotted blood (Fig. 3b, II), was clearly distinguished on CE-CTA and T_1-map. In addition, the T_1-map allowed to distinguish between the intraluminal and extraluminal flowing blood (II). In Patient no. 3, the T_1-map offered more detailed information on the content of the aneurysm sacs, whereas the perfused intraluminal of the endoprosthesis and the aneurysm sac are clearly visible on the CE-CTA and QISS-MRA images (Fig. 3c).

A detailed comparison between all imaging techniques is summarized in Table 3.

4. Discussion

After an EVAR procedure, follow ups are recommended 1, 6 and every 12 months after the intervention, for the entire life of the patient [4]. The use of DSA, CE-CTA, CE-US, and CE-MRA for diagnosing endoleaks was investigated in detail [5,6,9]. The application of DSA and CE-CTA is increasingly being avoided due to the significant radiation exposure and administration of nephrotoxic contrast-agent [24]. The CE-US is useful for detecting endoleaks in patients with abdominal aortic aneurysm (AAA) after EVAR [25], but not for thoracic aortic aneurysms, which are surrounded by bones and air-filled lungs (attenuation the transmission of the ultrasonic wave). CE-MRI offers superb anatomical contrast, but comes with some risk as well. In 2006, Grobner demonstrated an association between gadolinium and nephrogenic systemic fibrosis in 9 end stage renal disease patients [26]. In 2014, Kanda et al. reported the relationship between the increasing cumulative dose of a gadolinium-based contrast-agent and the high signal intensity in the brain in unenhanced T_1-weighted MRI [27].

The above concerns over MRI contrast-agent safety have spurred new developments in non-CE MRA-techniques. Saida et al. [28] presented a non-CE MRI method using motion-sensitized, driven equilibrium (MSDE)-prepared balanced turbo field echo (bTFE, bSSFP by Philips) for the detection and classification of type I–III endoleaks in in-vitro Endoleaks as well as flowing blood in the endoprosthesis were visualized with the subtraction of the flow-suppressed images from an identical acquisition without flow-suppression, so long as an appropriate VENC sensitivity value was used (2–20 cm/s [28]). In a further study, the feasibility of MSDE-bTFE was confirmed compared with CTA in 59 patients for thoracic-abdominal aortic, and common iliac arterial aneurysm [29].

Radial QISS-MRA has some advantages compared to MSDE-bTFE. First, it is less sensitive to motion and pulsation artefacts [10,16] and does not require careful adjustment of the VENC-setting. Second, all perfused areas in an imaging slice will be highlighted. Third, no subtraction of images with or without flow dephasing is required. Therefore, the measurement is shorter (~1 s/slice), image quality is not affected by the patient movement between successive data sets, and the measured spatial resolution is much higher than that of MSDE-bTFE.

Compared to CE-CTA and DSA, QISS-MRA allowed to visualize of endoprosthesis and localize of various types of endoleaks without use of contrast-agents and or harmful radiation, especially in complex vascular conditions as well as in endoleak types with slow flow rates. CE-CTA and QISS-MRA allowed to determine the aneurysm size due to their high spatial resolution and good image contrast for the differentiation between aneurysm content and dilated vessel wall. This is not the case for invasive DSA. While MRI is prone to artefacts from magnetic materials, only few were apparent on QISS-MRA. In fact, for some cases, the artefacts were stronger on CE-CTA images than on QISS-MRA. For type III, VI and V endoleaks, it was important to clarify the reason for the emergence of an aneurysm. In such cases, CE-CTA was not the method of choice, invasive DSA provided moderate to excellent results, QISS-MRA alone could not always be use, for example if dynamic information was required for the clarification of this clinical issue. In such cases, 4D-flow provided desirable information as an additional non-CE method.

Sakata et al. [30] used 4D-flow to assess the hemodynamics of type I–IV endoleaks in 31 patients after nitinol-based stent-graft deployment and compared the results to CTA. They reported that the 4D-flow was more sensitive than CE-CTA for detecting endoleaks, and that it allowed to divide type II endoleaks further into subcategories. Moreover, multiple concomitant endoleaks of different types were identified with 4D-

Table 2
Calculated hemodynamic relevant parameters in the aorta using GT-Flow. The measurement segments are displayed in Fig. 2a. The Wall shear stress is abbreviated to the WSS.

Flow parameter/position in the aorta	Segment 1	Segment 2	Segment 3
Velocity (cm/s)	43.4	76.9	48.9
WSS (N/m^2)	0.48	0.73	0.47

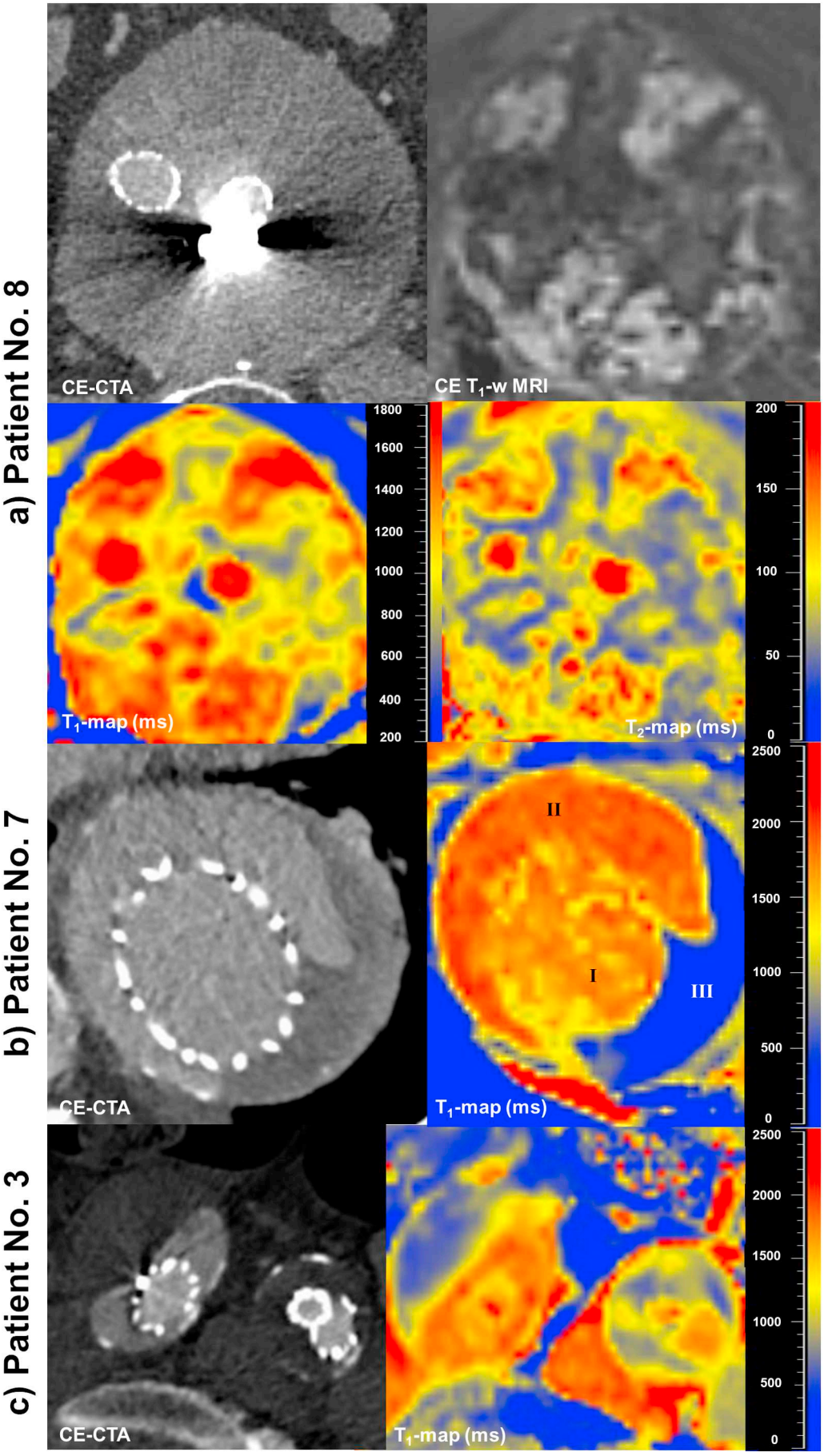

(caption on next page)

Fig. 3. Comparison between the CE-CTA and MRI for the investigation of the aneurysm sac content in three patients. The advanced types of endoleaks (IV, V) can be visualized using CE-CTA, if no image artefacts are present (a vs. b and c). Detailed information about the heterogeneous texture of the aneurysm sac can be provided using either CE-T_1-w MRI or non-CE T_1- and T_2-map.

flow in a single patient.

In our study, 4D-flow was used to investigate the aortic hemodynamics in two patients: one with a folded endoprosthesis and one with a continuously growing aneurysm sac. The 4D-flow MRI provided hemodynamics parameters such as the blood flow velocity, blood flow pressure and WSS. Compared to the physiological normal section of the aorta, elevated blood flow velocity and WSS were found in the stenosis [31,32].

The visualization of the blood flow and relative blood pressure were in good agreement with the invasive angiography. 4D-flow provided additional information on the WSS, which is not assessable using invasive angiography.

From our point of view, it is not easy to measure the blood flow in endoleaks with 4D-flow as presented by Sakata et al. [30], because the maximum blood flow velocity has to be known beforehand. For this reason, Sakata et al. acquired 2D-flow MRI and added a safety margin of 10 cm/s to the determined VENC. Here, the blood flow velocity of endoleaks type I–V was less than 20 cm/s. It is to be expected that at such a low blood flow value, the signal intensity may be affected by the background noise and the physiological movement of the aorta during the measurement. Sakata et al. performed 3D-CE-MRA before 4D-flow MRI, such that the signal-to-noise-ratio was increased due to the contrast agent. For the measurement of slow blood flow velocity, bipolar gradients are adjusted to achieve low VENC value. The lower VENC value corresponds to larger amplitudes of bipolar gradients, which generates more eddy currents and error of phases [33]. In presence of the flow turbulence, either an increased or a decreased flow parameter may be measured. If flow turbulence originates from normal physiological phenomenon, for example by the opening and the closing of the aortic valve, it is a part of the real flow, which is measured. On the other hand, flow-related turbulence can be a source of noise, if it is based on a pathological reason, for example due to an aortic valve or aortic arch stenosis.

We used T_1- and T_2-mapping for the pixel-wise analysis of the aneurysm sac in three patients with growing aneurysm sac. The metallic skeleton of the endoprosthesis was sharply delineated from the surrounding tissue on the T_1- and T_2-maps. The image quality on these maps was apparently not affected by the metal artefacts.

In the aneurysm sac, CE-CTA provided limited information about the heterogeneity of aneurysm content. Based on CE-CTA images, only perfused regions could be distinguished from clotted blood. T_1- and T_2-mapping allowed differentiation of more types of tissues based on the differences in their magnetic relaxation times. This information is particularly valuable for the assessment of heterogeneous content of aneurysms in patients with endoleak type IV and V. In contrast, invasive DSA was an unsuitable method for the clarification of changes in an aneurysmal sac. In general, a multi-focal biopsy after surgical revision or a *post-mortem* histological examination could be helpful for the clinical evaluation of T_1- and T_2-mapping results of the aneurysmal content.

5. Conclusion

In this work, four non-CE MRI techniques were used to image endovascular aortic prostheses, type I–V endoleaks, and aneurysm sacs. These results were compared to DSA and CE-CTA, as clinical standard methods, which are invasive/minimal-invasive methods and use ionizing radiation. The results indicate that non-CE MRI is promising for answering specific clinical questions in the framework of personalized diagnosis and post-procedural surveillance of patients with endovascular aortic prosthesis and a wide variety of endoleaks. The clinical impact of these MRI methods as a complementary or alternative modality to DSA and CE-CTA will be investigated in future studies involving a larger group of patients with aortic endoprosthesis.

Table 3
Comparison between CE-CTA, invasive angiography and MRI for answering specific clinical questions in the framework of personalized diagnosis and post-procedural surveillance of patients with EVAR based on the following criteria: + limited, + + moderate, + + + excellent, − unsuitable method. The expression "unsuitable" is used for a method, which is used in clinical routine for the answering advanced clinical question. However, this method cannot be considered as the method of choice for this purpose based on its insufficient image quality or contrast (for instance, DSA for the assessment of the heterogeneity of an aneurysm sac). An empty field means that this method is not used in general for the answering a special clinical question (for instance, 4D-flow MRI, T_1- and T_2-mapping for the measuring the size of aneurysm).

Patient	Type of endoleaks					Clinical indications	Clinical standard methods		MRI		
	I	II	III	IV	V		CE-CTA	Invasive angiography	QISS	4D-flow	T_1- and T_2-mapping
#1	x	x				1. Endoleak Ia and II	−	+	+		
						2. Influence of the TEVAR-stenosis	−	+ +		+ + +	
#2		x				1. Residual perfusion of a PAU in the aortic arch after TEVAR implantation	+	−	+		
#3	x	x				1. Endoleak Ib and II	+ + +	+ + +	+ + +		
						2. Heterogeneity of aneurysm content	+ +	−			+ + +
#4		x				1. Size of aneurysm	+ + +	−	+ + +		
						2. Endoleak II	+ + +	+ + +	+ + +		
#5		x				1. Clarify the presence of endoleak type II or III at the fenestration of the celiac trunk after abdominal endoprothesis with side branches.	+ +		+ + +		
#6			x			1. Reason for the continuously growing aneurysm sac	−	+ + +		+ + +	
						2. Position of the probably type III endoleak	+ + +	+ + +	+ +		
#7				x		1. Confirmation of the presence of endoleak type IV	+	+ + +	+		
						2. Size of aneurysm	+ + +	−	+ + +		
						3. Heterogeneity of aneurysm content	+	−			+ + +
#8					x (or new type of endoleak)	1. Reason for the continuously growing aneurysm sac	−	+ +	+ + +		
						2. Size of aneurysm	+ + +	−	+ + +		
						3. Heterogeneity of aneurysm content	+	−			+ + +

Declaration of Competing Interest

The authors declare that they have no conflict of interest.

References

[1] Parodi JC, Palmaz JC, Barone HD. Transfemoral intraluminal graft implantation for abdominal aortic aneurysms. Ann Vasc Surg 1991;5:491–9.
[2] Chen J, Stavropoulos SW. Management of endoleaks. Semin Intervent Radiol 2015;32:259–64.
[3] Bashir MR, Ferral H, Jacobs C, McCarthy W, Goldin M. Endoleaks after endovascular abdominal aortic aneurysm repair: management strategies according to CT findings. AJR Am J Roentgenol 2009;192:W178–86.
[4] Eskandari MK, Yao JS, Pearce WH, Rutherford RB, Veith FJ, Harris P, et al. Surveillance after endoluminal repair of abdominal aortic aneurysms. Cardiovasc Surg 2001;9:469–71.
[5] Habets J, Zandvoort HJA, Moll FL, Bartels LW, Vonken EPA, van Herwaarden JA, et al. Magnetic resonance imaging with a weak albumin binding contrast agent can reveal additional endoleaks in patients with an enlarging aneurysm after EVAR. Eur J Vasc Endovasc Surg 2015;50:331–40.
[6] Wacker FK, Valdeig S, Raatschen HJ, Meyer BC. C-arm CT—an adjunct to DSA for endoleak classification in patients with endovascular repair of abdominal aortic aneurysms. ROFO 2014;186:247–52.
[7] Kim M-H, Lee S-Y, Lee S-E, Yang M-S, Jung J-W, Park CM, et al. Anaphylaxis to iodinated contrast media: clinical characteristics related with development of anaphylactic shock. PLoS One 2014;9:e100154.
[8] Kanda T, Nakai Y, Oba H, Toyoda K, Kitajima K, Furui S. Gadolinium deposition in the brain. Magn Reson Imaging 2016;34:1346–50.
[9] Chung J, Kordzadeh A, Prionidis I, Panayiotopoulos Y, Browne T. Contrast-enhanced ultrasound (CEUS) versus computed tomography angiography (CTA) in detection of endoleaks in post-EVAR patients. Are delayed type II endoleaks being missed? A systematic review and meta-analysis. J Ultrasound 2015;18:91–9.
[10] Edelman RR, Silvers RI, Thakrar KH, Metzl MD, Nazari J, Giri S, et al. Nonenhanced MR angiography of the pulmonary arteries using single-shot radial quiescent-interval slice-selective (QISS): a technical feasibility study. J Cardiovasc Magn Reson 2017;19:48.
[11] Edelman RR, Giri S, Pursnani A, Botelho MPF, Li W, Koktzoglou I. Breath-hold imaging of the coronary arteries using Quiescent-Interval Slice-Selective (QISS) magnetic resonance angiography: pilot study at 1.5 Tesla and 3 Tesla. J Cardiovasc Magn Reson 2015;17:101.
[12] Markl M, Chan FP, Alley MT, Wedding KL, Draney MT, Elkins CJ, et al. Time-resolved three-dimensional phase-contrast MRI. J Magn Reson Imaging 2003;17:499–506.
[13] Frydrychowicz A, Berger A, Russe MF, Stalder AF, Harloff A, Dittrich S, et al. Time-resolved magnetic resonance angiography and flow-sensitive 4-dimensional magnetic resonance imaging at 3 Tesla for blood flow and wall shear stress analysis. J Thorac Cardiovasc Surg 2008;136:400–7. https://doi.org/10.1016/j.jtcvs.2008.02.062.
[14] Stankovic Z, Allen BD, Garcia J, Jarvis KB, Markl M. 4D flow imaging with MRI. Cardiovasc Diagn Ther 2014;4:173–92. https://doi.org/10.3978/j.issn.2223-3652.2014.01.02.
[15] Edelman RR, Sheehan JJ, Dunkle E, Schindler N, Carr J, Koktzoglou I. Quiescent-interval single-shot unenhanced magnetic resonance angiography of peripheral vascular disease: technical considerations and clinical feasibility. Magn Reson Med 2010;63:951–8.
[16] Edelman RR, Giri S, Dunkle E, Galizia M, Amin P, Koktzoglou I. Quiescent-inflow single-shot magnetic resonance angiography using a highly undersampled radial k-space trajectory. Magn Reson Med 2013;70:1662–8.
[17] Hamilton-Craig CR, Strudwick MW, Galloway GJ. T_1 mapping for myocardial fibrosis by cardiac magnetic resonance relaxometry—a comprehensive technical review. Frontiers in Cardiovascular Medicine 2016;3:49.
[18] Montant P, Sigovan M, Revel D, Douek P. MR imaging assessment of myocardial edema with T_2 mapping. Diagn Interv Imaging 2015;96:885–90.
[19] Yu AC, Badve C, Ponsky LE, Pahwa S, Dastmalchian S, Rogers M, et al. Development of a combined MR fingerprinting and diffusion examination for prostate cancer. Radiology 2017;283:729–38.
[20] Wigstrom L, Sjoqvist L, Wranne B. Temporally resolved 3D phase-contrast imaging. Magn Reson Med 1996;36:800–3.
[21] Burris NS, Hope MD. 4D flow MRI applications for aortic disease. Magn Reson Imaging Clin N Am 2015;23:15–23.
[22] Zhang X, Petersen ET, Ghariq E, de Vis JB, Webb AG, Teeuwisse WM, et al. In vivo blood T_1 measurements at 1.5 T, 3 T, and 7 T. Magn Reson Med 2013;70:1082–6.
[23] Barth M, Moser E. Proton NMR relaxation times of human blood samples at 1.5 T and implications for functional MRI. Cell Mol Biol (Noisy-le-Grand) 1997;43:783–91.
[24] Partovi S, Trischman T, Rafailidis V, Ganguli S, Rengier F, Goerne H, et al. Multimodality imaging assessment of endoleaks post-endovascular aortic repair. Br J Radiol 2018;91:20180013.
[25] Iezzi R, Basilico R, Giancristofaro D, Pascali D, Cotroneo AR, Storto ML. Contrast-enhanced ultrasound versus color duplex ultrasound imaging in the follow-up of patients after endovascular abdominal aortic aneurysm repair. J Vasc Surg 2009;49:552–60.
[26] Grobner T. Gadolinium—a specific trigger for the development of nephrogenic fibrosing dermopathy and nephrogenic systemic fibrosis? Nephrol Dial Transplant 2006;21:1104–8.
[27] Kanda T, Ishii K, Kawaguchi H, Kitajima K, Takenaka D. High signal intensity in the dentate nucleus and globus pallidus on unenhanced T1-weighted MR images: relationship with increasing cumulative dose of a gadolinium-based contrast material. Radiology 2014;270:834–41.
[28] Saida T, Mori K, Yabe H, Shindo M, Nasu K, Shiigai M, et al. Noninvasive visualization of endoleaks after endovascular aortic aneurysm repair through unenhanced MRI with motion-sensitized driven equilibrium preparation: phantom experiments. J Magn Reson Imaging 2013;38:714–21.
[29] Mori K, Saida T, Sato F, Uchikawa Y, Konishi T, Ishiguro T, et al. Endoleak detection after endovascular aneurysm repair using unenhanced MRI with flow suppression technique: feasibility study in comparison with contrast-enhanced CT. Eur Radiol 2017;27:336–44.
[30] Sakata M, Takehara Y, Katahashi K, Sano M, Inuzuka K, Yamamoto N, et al. Hemodynamic analysis of endoleaks after endovascular abdominal aortic aneurysm repair by using 4-dimensional flow-sensitive magnetic resonance imaging. Circ J 2016;80:1715–25.
[31] Nilkantha Kirubha A. Karthikaeditor. Identification of stenosis in coronary arteries using velocity and wall shear stress analysis. 2017.
[32] Knobelsdorff-Brenkenhoff F von, Karunaharamoorthy A, Trauzeddel RF, Barker AJ, Blaszczyk E, Markl M, Schulz-Menger J. Evaluation of aortic blood flow and wall shear stress in aortic stenosis and its association with left ventricular remodeling. Circ Cardiovasc Imaging 2016; 9: e004038-e004038.
[33] Zhou Y, Wolff SD, Grist TM, Polzin JA. Investigation of Eddy current effects on phase contrast imaging. 11th proc. intl. soc. mag. reson. med. 2004.